

Vibrational Perturbation of the [FeFe] Hydrogenase H-Cluster Revealed by $^{13}\text{C}^2\text{H}$ -ADT Labeling

Vladimir Pelmeshnikov, James A. Birrell,* Leland B. Gee, Casseday P. Richers, Edward J. Reijerse, Hongxin Wang, Simon Arragain, Nakul Mishra, Yoshitaka Yoda, Hiroaki Matsuura, Lei Li, Kenji Tamasaku, Thomas B. Rauchfuss,* Wolfgang Lubitz, and Stephen P. Cramer*



Cite This: *J. Am. Chem. Soc.* 2021, 143, 8237–8243



Read Online

ACCESS |



Metrics & More



Article Recommendations



Supporting Information

ABSTRACT: [FeFe] hydrogenases are highly active catalysts for the interconversion of molecular hydrogen with protons and electrons. Here, we use a combination of isotopic labeling, ^{57}Fe nuclear resonance vibrational spectroscopy (NRVS), and density functional theory (DFT) calculations to observe and characterize the vibrational modes involving motion of the 2-azapropane-1,3-dithiolate (ADT) ligand bridging the two iron sites in the $[2\text{Fe}]_{\text{H}}$ subcluster. A $^{-13}\text{C}^2\text{H}_2$ -ADT labeling in the synthetic diiron precursor of $[2\text{Fe}]_{\text{H}}$ produced isotope effects observed throughout the NRVS spectrum. The two precursor isotopologues were then used to reconstitute the H-cluster of [FeFe] hydrogenase from *Chlamydomonas reinhardtii* (CrHydA1), and NRVS was measured on samples poised in the catalytically crucial H_{hyd} state containing a terminal hydride at the distal Fe site. The $^{13}\text{C}^2\text{H}$ isotope effects were observed also in the H_{hyd} spectrum. DFT simulations of the spectra allowed identification of the ^{57}Fe normal modes coupled to the ADT ligand motions. Particularly, a variety of normal modes involve shortening of the distance between the distal Fe–H hydride and ADT N–H bridgehead hydrogen, which may be relevant to the formation of a transition state on the way to H_2 formation.

Molecular hydrogen is viewed as an ideal carbon-free energy carrier that could be part of a transition to a sustainable economy without CO_2 emissions.^{1,2} At the moment, the majority of industrial hydrogen is produced by high-temperature steam reforming of natural gas which leads to the release of at least one molecule of CO_2 for every 4 H_2 produced.³ Ideally, electrochemical energy from solar, wind, or other carbon-free sources could be used to drive the water-splitting or “hydrogen evolution reaction” (HER) without CO_2 release.^{4,4} Highly efficient catalysts with low overpotentials are essential for electrochemical conversions of hydrogen, and the high prices and scarcity of the current Pt or other noble metal HER catalysts have led to the search for systems that use earth-abundant materials.^{5–7} One source of inspiration driving this search is Nature, which uses plentiful transition metals Fe or Fe with Ni in the active sites of hydrogenases.^{8,9}

Hydrogenases are enzymes that catalyze the reversible interconversion of molecular hydrogen with protons and electrons: $\text{H}_2 \rightleftharpoons 2\text{H}^+ + 2\text{e}^-$. [FeFe] hydrogenases contain an active site “H-cluster” consisting of a $[4\text{Fe}-4\text{S}]_{\text{H}}$ cluster linked via a cysteine residue to a unique $[2\text{Fe}]_{\text{H}}$ subcluster (Figure 1a).¹¹ This subcluster carries a 2-azapropane-1,3-dithiolate (ADT) ligand bridging a pair of CO and CN^- ligated Fe ions. The ADT bridgehead nitrogen has been implicated as part of a proton transfer relay extending through a neighboring cysteine.^{12–16} In the *Chlamydomonas reinhardtii* [FeFe] hydrogenase (CrHydA1), the conserved relay consists of C169, a water molecule, and oxygens from E141, S189, and E144 residues.

An iron hydride form of [FeFe] hydrogenase, H_{hyd} , is a key intermediate of the catalytic cycle, and it has been studied by

multiple spectroscopic and molecular modeling techniques.^{17–24} The H_{hyd} species contains a terminal $\text{Fe}_d\text{-H}_h$ (hydride) at the $[2\text{Fe}]_{\text{H}}$ iron site distal to $[4\text{Fe}-4\text{S}]_{\text{H}}$ (Figure 1b), with a $[4\text{Fe}-4\text{S}]_{\text{H}}^+ \text{-Fe}_p(\text{II})\text{Fe}_d(\text{II})$ redox state for the H-cluster, along with the $-\text{NH}_{\text{ADT}}-$ amine form of the ADT bridgehead.^{18–21}

Nuclear resonance vibrational spectroscopy (NRVS) has become a popular technique for elucidating the element-selective normal modes of appropriate Mössbauer isotopes.^{25–31} In previous work on the CrHydA1 and DdHydAB (from *Desulfovibrio desulfuricans*) enzymes,^{20–22} we have shown that $^{57}\text{Fe}_d\text{-H}_h$ bending modes can be observed using ^{57}Fe -NRVS for the H_{hyd} species and that these modes exhibit peak positions that are characteristic of the local environment. To better identify additional normal modes of H_{hyd} , we proceeded to label the $[2\text{Fe}]_{\text{H}}$ subcluster not only with ^{57}Fe but also with ^{13}C and D in the methylene groups of the ADT ligand. We accomplished this by preparing a $[2\text{Fe}]_{\text{H}}$ precursor, the ^{57}Fe -labeled salt $(\text{Et}_4\text{N})_2[^{57}\text{Fe}_2[(\text{SCH}_2)_2\text{NH}](\text{CN})_2(\text{CO})_4]$ (1) as well as its variant also labeled with ^{13}C and D on the two methylene groups of the ADT ligand ($^{13}\text{CD-1}$).³² We then used these samples to reconstitute an apo form of CrHydA1 containing the $[4\text{Fe}-4\text{S}]_{\text{H}}$ cluster but lacking the $[2\text{Fe}]_{\text{H}}$ subsite.³³

Received: March 3, 2021

Published: May 27, 2021



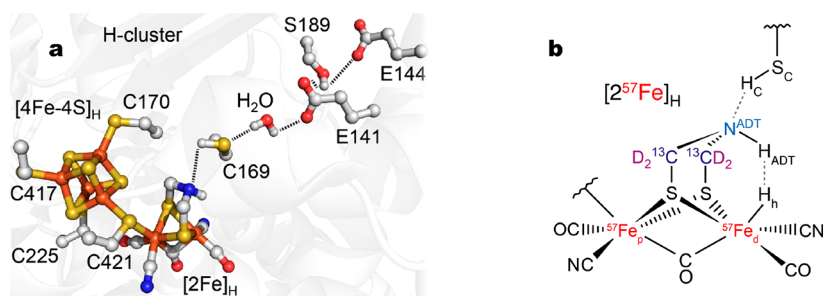


Figure 1. (a) [FeFe] hydrogenase active site including key amino acids in the proton transfer pathway (based on the PDB 4XDC¹⁰ structure of the Cpl enzyme from *Clostridium pasteurianum*, but using CrHydA1 sequence numbering). (b) Schematic structure of the [2Fe]_H subcluster in the H_{hyd} state, showing the isotopically labeled nuclei ⁵⁷Fe, ¹³C, and D (i.e. ²H). The important hydrogens, H_h (catalytic hydride at the distal Fe_d iron), H_{ADT} (at the ADT N_{ADT} nitrogen), and H_c (at the S_C C169 sulfur), are shown.

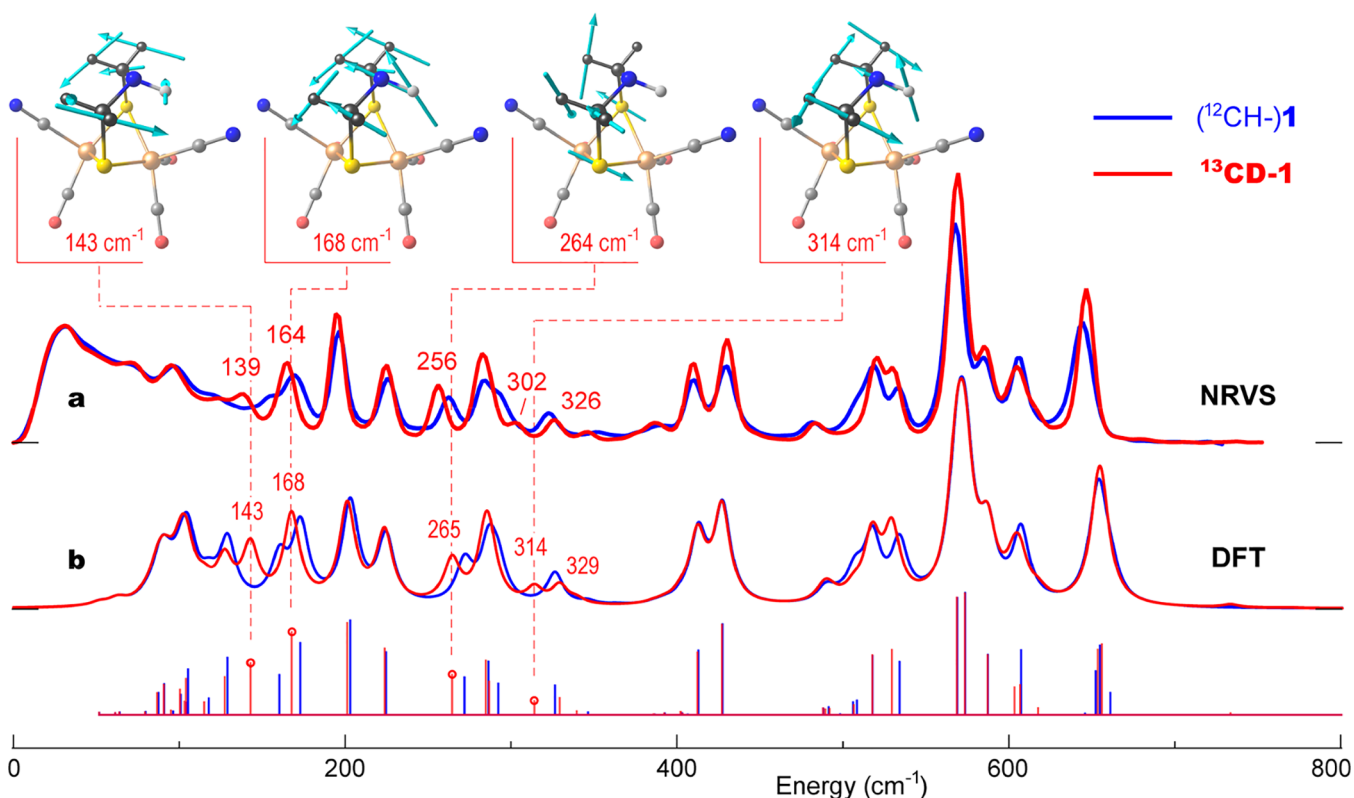


Figure 2. ⁵⁷Fe-PVDOS for the [2Fe]_H precursor isotopologues **1** (blue) vs ¹³CD-**1** (red) from (a) NRVS experiments and (b) DFT calculations. Sticks correspond to individual DFT normal mode energies and intensities before lineshape convolution. For ¹³CD-**1**, important band positions are labeled, and atomic motions in selected normal modes are shown.

We first examine NRVS spectra for the precursor isotopologues **1** vs ¹³CD-**1** in Figure 2a. Close inspection reveals a number of subtle changes to band positions and intensities in the broad ~100–700 cm⁻¹ range, most of them well reproduced by the DFT simulation shown in Figure 2b. We note that this is the first demonstration of NRVS isotope shifts from labeling in the second and third coordination spheres of ⁵⁷Fe, although such shifts have been seen before in resonance Raman spectra.^{34,35} In the following, when referring to the bands observed (or vibrational frequencies calculated) for the two isotopologues, we use a nomenclature $x \rightarrow y$ (cm⁻¹) where x and y represent **1** and ¹³CD-**1**, respectively.

Since the bands from 400 to 660 cm⁻¹ are dominated by Fe–CN and Fe–CO motions, we focus instead on differences in the region from 100 to 350 cm⁻¹, which contains delocalized bending and torsional modes as well as Fe–S stretching. In the

¹³CD-**1** spectra, several bands exhibit clear downshifts from the (¹²CH-)**1** data, for example, at 150 → 139, 168 → 164, and 260 → 256 cm⁻¹ (Figure 2a). This pattern is echoed in the ¹³CD-**1** DFT simulations, with downshifted bands at 161 → 143, 173 → 168, and 273 → 265 cm⁻¹ (Figure 2b). The normal-mode analysis also reveals an isotope-dependent redistribution of the intensities underlying the DFT bands at 326 → 329/314 cm⁻¹, mapping onto the NRVS features at 322 → 326/302 cm⁻¹.

Having identified the most significant isotope shifts in the precursor spectra, we now illustrate the atomic motions deduced from the DFT calculations. As displayed in Figure 2 for ¹³CD-**1**, the normal mode calculated at 143 cm⁻¹ is mostly out-of-phase rotation of the two ADT –μS¹³CD₂– groups around their S–C axes, combined with some motion of the μS pivot points due to Fe–S–Fe bending (see animated

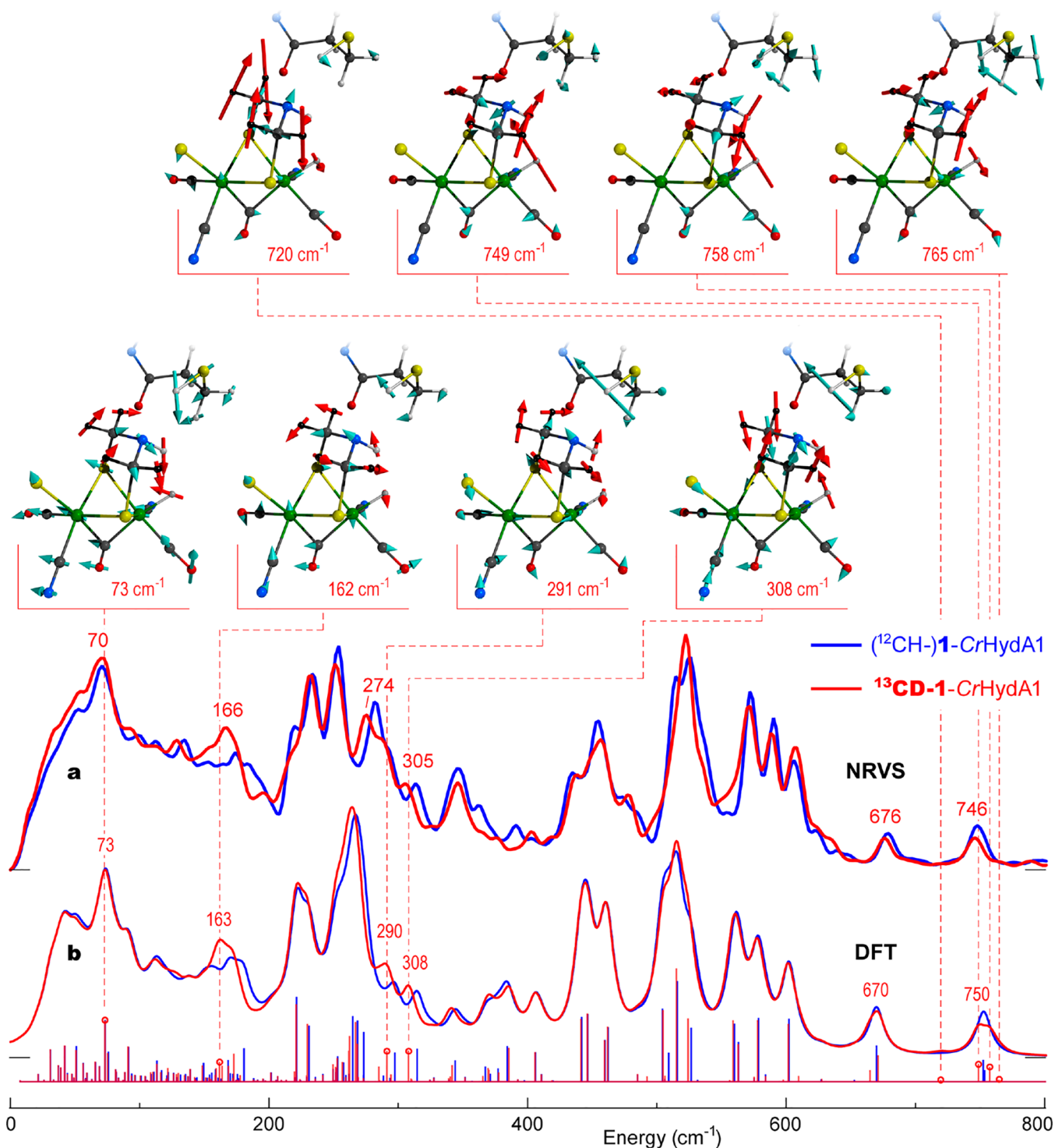


Figure 3. ^{57}Fe -PVDOS for the H_{hyd} state isotopologues 1-CrHydA1 (blue) vs $^{13}\text{CD-1-CrHydA1}$ (red) from (a) an NRVS experiment and (b) DFT calculations. Sticks correspond to individual DFT normal mode energies and intensities before broadening. For $^{13}\text{CD-1-CrHydA1}$, important band positions are labeled, and atomic motions in selected normal modes are shown. Only the $[\text{2Fe}]_{\text{H}}$ and C169 fragments of the DFT model are shown with the methylene, H_{br} , and H_{ADT} hydrogen nuclei displacements indicated by red arrows.

representations of the calculated vibrational modes as part of the Supporting Information and their characterization in Table S2). The large amount of methylene motion explains the significant isotope shift. In contrast, the 168 cm^{-1} mode involves rocking of the entire $-\text{D}_2^{13}\text{C}-\text{NH}-^{13}\text{CD}_2-$ assembly in one direction while the underlying Fe_2S_2 cluster (and associated ligands) rotates in the opposite direction. At higher

frequencies, the 264 cm^{-1} mode involves out-of-phase displacements of the $-\mu\text{S}^{13}\text{CD}_2-$ fragments with substantial Fe–S stretching character, while the 314 cm^{-1} mode is an in-phase $^{13}\text{CD}_2-$ methylene group motion, accompanied by wagging of the $-\text{NH}-$ bridgehead in the opposite direction.

Our key observations from these precursor studies are (i) that the ^{13}CD substitution in the Fe-bridging ADT ligand

induces measurable isotope shifts in the ^{57}Fe NRVS spectra, on the order of the 8 cm^{-1} instrumental resolution; (ii) that the DFT calculations are sufficiently accurate to reproduce these shifts, allowing confidence in the motions assigned to these modes; and (iii) that the calculations predict a variety of ADT flexing modes with significant motion of the $-\text{NH}-$ bridgehead.

Precursors **1** and $^{13}\text{CD-1}$ were used for maturation of the apo CrHydA1 containing natural-abundance Fe in the $[\text{4Fe-4S}]_{\text{H}}$ cluster. This yielded holo CrHydA1 labeled with ^{57}Fe in the $[\text{2Fe}]_{\text{H}}$ subcluster, and with either a natural-abundance ADT ligand (**1-CrHydA1**) or $^{-13}\text{CD}_2-$ in the methylene portions of ADT ($^{13}\text{CD-1-CrHydA1}$). These samples were poised in the H_{hyd} state by reduction with 100 mM sodium dithionite at pH 6. As shown by infrared (IR) spectra in Figure S1, both samples exhibited the standard H_{hyd} IR signature, with minimal contributions from other redox states.

NRVS data for **1-CrHydA1** and $^{13}\text{CD-1-CrHydA1}$ are shown in Figure 3a, with the corresponding DFT simulations in Figure 3b. The calculated spectra were generated using a DFT model of H_{hyd} including the entire H-cluster and its immediate protein environment;^{21,22,36} see DFT methods and model coordinates in the Supporting Information for further details. Again, we focus first on differences in the low-energy region, where we see the most obvious isotope effects. These include NRVS downshifts at $281 \rightarrow 274$ and $313 \rightarrow 305\text{ cm}^{-1}$, with the DFT simulations yielding corresponding modifications at $296 \rightarrow 290$ and $314 \rightarrow 308\text{ cm}^{-1}$. The $150\text{--}200\text{ cm}^{-1}$ isotope-dependent NRVS region ($\sim 174 \rightarrow 166\text{ cm}^{-1}$) of H_{hyd} essentially repeats in the DFT spectra ($\sim 171 \rightarrow 163\text{ cm}^{-1}$), indicating overlapping contributions from different modes. A complementary DFT simulation for the $[\text{4Fe-4S}]_{\text{H}}^{2+}-\text{Fe}_{\text{p}}(\text{II})-\text{Fe}_{\text{d}}(\text{I})$ redox state of the H-cluster, H_{ox} , reveals comparable $^{12}\text{CH} \rightarrow ^{13}\text{CD}$ spectral shifts in the broader $\sim 150\text{--}330\text{ cm}^{-1}$ region (Figure S2); this indicates that the ADT labeling effects observed in NRVS are stable against potential impurities from additional redox states of the H-cluster.

The atomic motions deduced from the DFT calculations on H_{hyd} are displayed in Figure 3 and animated as part of the Supporting Information. The 162 cm^{-1} band of $^{13}\text{CD-1-CrHydA1}$ contains $[\text{2Fe}]_{\text{H}}$ modes heavily mixed with the protein environment, but an important feature here is rocking of the $-\text{NH}_{\text{ADT}}-$ bridgehead toward the distal iron hydride $\text{Fe}_{\text{d}}-\text{H}_{\text{h}}$, along with out-of-phase rotation of the ADT $^{-13}\text{CD}_2-$ groups; this character matches the $^{13}\text{CD-1}$ precursor mode at 143 cm^{-1} . At higher energies, the 291 cm^{-1} mode exhibits a breathing motion of the Fe_2S_2 moiety, which leads to changing the distance between Fe_{p} and the $[\text{4Fe-4S}]_{\text{H}}$ cluster; in this case, there is an in-phase motion of the ADT methylene groups in the opposite direction of the amine bridgehead, similar to the $^{13}\text{CD-1}$ mode at 314 cm^{-1} described above. The 308 cm^{-1} mode exhibits an entire ADT fragment wagging/rotation relative to Fe_{p} and Fe_{d} , equivalent to the $^{13}\text{CD-1}$ mode at 287 cm^{-1} . We also illustrate the 73 cm^{-1} mode, which is highly delocalized with torsional motions of the entire H-cluster.

We now turn to the higher-energy side of the H_{hyd} spectra, which contains two distinct $\text{Fe}_{\text{d}}-\text{H}_{\text{h}}$ bending mode peaks observed at $679/676$ and $748/746\text{ cm}^{-1}$, and calculated at $670/670$ and $753/750\text{ cm}^{-1}$ (Figure 3). These were the focus of previous studies because they characterize the terminal iron hydride bonding and its interactions with the surround-

ings.^{20–22} The two main features arise from the relatively pure H_{h} hydride bending motion perpendicular to and parallel to the plane defined by the $\text{Fe}_{\text{p}}-\text{Fe}_{\text{d}}$ axis and the $\text{Fe}_{\text{d}}-\text{H}_{\text{h}}$ bond, respectively. Although the isotope-dependent shifts in these bands are small and nearly unmeasurable, the fine structure of the underlying normal modes displays a difference. In the current DFT analysis there are **1- $^{13}\text{CD-1-CrHydA1}$** “perpendicular” modes at $670/665, 671\text{ cm}^{-1}$, and “parallel” modes at $752, 754/749, 758\text{ cm}^{-1}$ respectively. The ^{13}CD -labeling introduces $\text{N}_{\text{ADT}}-\text{H}_{\text{ADT}}$ bending admixtures to the $\text{Fe}_{\text{d}}-\text{H}_{\text{h}}$ modes, where the H_{ADT} and H_{h} nuclei displace either in- or out-of-phase; e.g., the 758 cm^{-1} “parallel” mode (Figure 3) brings H_{h} and H_{ADT} closer during half of each excursion cycle. The calculations suggest an increased involvement of the heavier ^{13}CD -ADT fragment in the $\text{Fe}_{\text{d}}-\text{H}_{\text{h}}$ bends, with rotations of the two $^{-13}\text{CD}_2-$ methylene groups contributing at least 16% to the vibrational kinetic energy. Similar modes are calculated in the ADT-labeled $^{13}\text{CD-1}$ precursor in the $\sim 670\text{--}770\text{ cm}^{-1}$ region, while the unlabeled ($^{12}\text{CH-}$)**1** variant produces their counterparts at frequencies only above 800 cm^{-1} (Table S2).

The DFT analysis therefore indicates that some modes in the $\text{Fe}_{\text{d}}-\text{H}_{\text{h}}$ bending region involve mixing with motions inherent to the ^{13}CD -labeled ADT ligand. A search for such “satellite” modes is what initially prompted our isotopic labeling investigation. The experimental data might show weak “satellite” features on either side of the main $\text{Fe}_{\text{d}}-\text{H}_{\text{h}}$ bending peaks (Figure 3). However, despite prolonged data collection in this region to improve the signal-to-noise (S/N) ratio, firm assignment of the small differences to “satellites” is not yet possible. The exact calculated energies of the “satellites” should also be taken with caution, because they are governed by motion of a very light H_{h} nucleus that mediates interaction between $^{57}\text{Fe}_{\text{d}}$ and the ADT bridgehead. Further experimental insight into these modes will require a significantly higher NRVS photon flux, which may be available in the next generation of synchrotron sources, e.g., PETRA-IV.³⁷

The accuracy of the DFT calculations at reproducing the experimental NRVS spectra of the unlabeled and isotopically labeled precursor and $[\text{2Fe}]_{\text{H}}$, here and in our previous work,^{20–22,36} gives us confidence that it is valuable to consider the predicted “satellite” modes in H_{hyd} , whether or not they can be conclusively detected by NRVS. Illustrations of these “satellite” modes at 720 and 765 cm^{-1} are included in Figure 3. The latter two modes involve “parallel” $\text{Fe}_{\text{d}}-\text{H}_{\text{h}}$ bending, similar to the 749 and 758 cm^{-1} modes. Interestingly, some of these modes involve motion of the nearby cysteine at the end of the proton transfer channel leading to the ADT ligand. These vibrational modes appear to represent a pathway for coupled proton transfer from $(\text{C169})\text{S}_{\text{C}}-\text{H}_{\text{C}}$ to N_{ADT} and from $\text{N}_{\text{ADT}}-\text{H}_{\text{ADT}}$ to $\text{Fe}_{\text{d}}-\text{H}_{\text{h}}$.

Are any other modes relevant to H_2 production catalysis? We inspected the DFT calculations for changes in $\text{H}_{\text{ADT}}\cdots\text{H}_{\text{h}}$ and $\text{N}_{\text{ADT}}\cdots\text{H}_{\text{C}}$ distances that occur during normal mode displacements (see Figure S3). The results for the modes with the greatest distance changes are summarized in Table S1. The equilibrium 2.06 \AA $\text{H}_{\text{ADT}}\cdots\text{H}_{\text{h}}$ distance is already firmly in the $1.7\text{--}2.2\text{ \AA}$ range for a “dihydrogen bond”,³⁸ and it is similar to the 2.02 \AA value seen as the shortest $\text{H}\cdots\text{H}$ distance in solid BH_3NH_3 .³⁹ We found that a few modes contribute a disproportionate amount of motion involving the $\text{H}_{\text{ADT}}\cdots\text{H}_{\text{h}}$ distance as well as the $\text{N}_{\text{ADT}}\cdots\text{H}_{\text{C}}$ distance. In particular, the “parallel” $\text{Fe}_{\text{d}}-\text{H}_{\text{h}}$ bending modes at $752/758\text{ cm}^{-1}$ yield the

record $\sim 0.14/0.15$ Å contractions in the $H_{\text{ADT}}\cdots H_{\text{h}}$ distance across the entire vibrational spectra. For the $N_{\text{ADT}}\cdots H_{\text{C}}$ distance, the largest vibrational contraction of ~ 0.11 Å is achieved in the $S_{\text{C}}-H_{\text{C}}$ stretching mode calculated at $2449/2449$ cm^{-1} .

From time-resolved photochemical IR studies, Sanchez et al. have shown that the decay of H_{hyd} is kinetically competent as a near-final step in the [FeFe] hydrogenase catalytic cycle.⁴⁰ However, since the pK_{a} for a neutral secondary amine such as the ADT bridgehead nitrogen is extremely high, an intervening protonated ADT $-NH_2^+$ intermediate, $H_{\text{hyd}}H^+$, has often been included in the catalytic cycle.^{17,24,41-44} Our results, which document the role of ADT flexibility in normal modes that bring H_{ADT} and H_{h} closer together, offer the possibility of a mechanism update.

In this speculative scenario, high-frequency modes such as at $752/758$ and $2449/2449$ cm^{-1} , combined with low-frequency modes such as at 73 cm^{-1} , would involve coordinated motion of H_{ADT} toward H_{h} , while H_{C} moves toward N_{ADT} . This might precipitate a “deep tunneling” transfer of H_{ADT} to H_{h} , while $S_{\text{C}}-H_{\text{C}}$ transfer replenishes the $N_{\text{ADT}}-H_{\text{ADT}}$, and with the $S_{\text{C}}-H_{\text{C}}$ proton reloaded from the H_2O in the proton transfer chain. Champion and co-workers have shown that deep tunneling can allow high pK_{a} residues to participate in proton transfer chains, as invoked for a serine residue in the green fluorescent protein.⁴⁵ If the transfer reaction for H_{hyd} were facilitated by electron transfer from the $[4\text{Fe}-4\text{S}]_{\text{H}}^+$ to the $[\text{Fe}^{\text{II}}\text{Fe}^{\text{II}}]_{\text{H}}$ subsite, the overall PCET reaction would yield an H_{ox} electronic state with bound H_2 . This scenario agrees with calculations on the reverse reaction of H_2 activation by Greco et al.⁴⁶

In summary, we have investigated vibrations of the [FeFe] hydrogenase active site in the H_{hyd} state through ^{57}Fe , ^{13}C , and D isotopic labeling, combined with ^{57}Fe NRVS measurements and DFT calculations. This represents the first observation of second and third coordination sphere isotope effects using NRVS. We identified normal modes involving the flexing of the bridging ADT ligand that point to its unique properties as an active site ligand. The combined motions of the $\text{Fe}_{\text{d}}-H_{\text{h}}$, $N_{\text{ADT}}-H_{\text{ADT}}$, and $(\text{C}169)S_{\text{C}}-H_{\text{C}}$ protons are presumably coupled to the remainder of the proton transfer chain as well as electron transfer. These effects may be important for catalysis and will be investigated in future studies.

■ ASSOCIATED CONTENT

SI Supporting Information

The Supporting Information is available free of charge at <https://pubs.acs.org/doi/10.1021/jacs.1c02323>.

Experimental and computational procedures and additional data and figures including FTIR spectra, ^{57}Fe -PVDOS results, and relative displacements (PDF)

Animated vibrational modes of the H_{hyd} DFT model as GIF files (ZIP)

Animated vibrational modes of the precursor DFT model as GIF files (ZIP)

Coordinates of the precursor, H_{hyd} , and H_{ox} DFT models as XYZ files (ZIP)

■ AUTHOR INFORMATION

Corresponding Authors

James A. Birrell – Max Planck Institute for Chemical Energy Conversion, 45470 Mülheim an der Ruhr, Germany;

orcid.org/0000-0002-0939-0573; Email: james.birrell@cec.mpg.de

Thomas B. Rauchfuss – School of Chemical Sciences, University of Illinois, Urbana, Illinois 61801, United States;

orcid.org/0000-0003-2547-5128; Email: rauchfuz@illinois.edu

Stephen P. Cramer – SETI Institute, Mountain View, California 94043, United States; orcid.org/0000-0002-3751-7623; Email: scramer@seti.org

Authors

Vladimir Pelmeshchikov – Institut für Chemie, Technische Universität Berlin, 10623 Berlin, Germany; orcid.org/0000-0002-0523-4418

Leland B. Gee – Department of Chemistry, Stanford University, Stanford, California 94305, United States; orcid.org/0000-0002-5817-3997

Casseday P. Richers – School of Chemical Sciences, University of Illinois, Urbana, Illinois 61801, United States; orcid.org/0000-0002-1324-0447

Edward J. Reijerse – Max Planck Institute for Chemical Energy Conversion, 45470 Mülheim an der Ruhr, Germany; orcid.org/0000-0001-9605-4510

Hongxin Wang – SETI Institute, Mountain View, California 94043, United States; orcid.org/0000-0002-7325-0161

Simon Arragain – IFP Energies nouvelles, 92852 Rueil-Malmaison, France; Department of Chemistry, University of California, Davis, California 95616, United States; orcid.org/0000-0002-6500-0066

Nakul Mishra – Department of Chemistry, University of California, Davis, California 95616, United States; orcid.org/0000-0003-4382-933X

Yoshitaka Yoda – Precision Spectroscopy Division, SPring-8/JASRI, Sayo, Hyogo 679-5198, Japan; orcid.org/0000-0003-3062-8651

Hiroaki Matsuura – Life Science Research Infrastructure Group, Advanced Photon Technology Division, RIKEN/SPring-8 Center, Sayo, Hyogo 679-5148, Japan; orcid.org/0000-0002-8659-9952

Lei Li – Hyogo Science and Technology Association, Synchrotron Radiation Research Center, Tatsuno-shi, Hyogo 679-5165, Japan; orcid.org/0000-0001-7909-6487

Kenji Tamasaku – Research and Utilization Division, SPring-8/JASRI, Sayo, Hyogo 679-5198, Japan; orcid.org/0000-0003-1440-0518

Wolfgang Lubitz – Max Planck Institute for Chemical Energy Conversion, 45470 Mülheim an der Ruhr, Germany; orcid.org/0000-0001-7059-5327

Complete contact information is available at: <https://pubs.acs.org/doi/10.1021/jacs.1c02323>

Notes

The authors declare no competing financial interest.

■ ACKNOWLEDGMENTS

V.P. acknowledges funding by the Deutsche Forschungsgemeinschaft (DFG, German Research Foundation) under Germany's Excellence Strategy, EXC 2008-390540038, UniSysCat. J.A.B. acknowledges funding from the DFG SPP 1927 “Iron-Sulfur for Life” project (Project BI 2198/1-1). E.J.R., J.A.B., and W.L. would like to thank the Max Planck Society for continuous financial support. The contributions of T.B.R. and C.P.R. were funded by the U.S. National Institutes

of Health through GM61153. S.P.C. was funded by NIH GM65440. Some computational work was performed under the XSIM project on the CORI computing system at NERSC, a U.S. Department of Energy Office of Science User Facility operated under Contract DE-AC02-05CH11231. The authors gratefully acknowledge the assistance by Giorgio Caserta in acquisition of the NRVS data.

REFERENCES

- (1) Glenk, G.; Reichelstein, S. Economics of converting renewable power to hydrogen. *Nat. Energy* **2019**, *4* (3), 216–222.
- (2) Armaroli, N.; Balzani, V. The Hydrogen Issue. *ChemSusChem* **2011**, *4* (1), 21–36.
- (3) Avila Neto, C.; Dantas, S. C.; Silva, F. A.; Franco, T. V.; Romanielo, L.; Hori, C.; Assis, A. J. Hydrogen production from methane reforming: Thermodynamic assessment and autothermal reactor design. *J. Nat. Gas Sci. Eng.* **2009**, *1*, 205–215.
- (4) Hosseini, S. E.; Wahid, M. A. Hydrogen from solar energy, a clean energy carrier from a sustainable source of energy. *Int. J. Energy Res.* **2020**, *44* (6), 4110–4131.
- (5) Ren, X. F.; Lv, Q. Y.; Liu, L. F.; Liu, B. H.; Wang, Y. R.; Liu, A. M.; Wu, G. Current progress of Pt and Pt-based electrocatalysts used for fuel cells. *Sust. En. Fuels* **2020**, *4* (1), 15–30.
- (6) Bullock, R. M.; Helm, M. L. Molecular Electrocatalysts for Oxidation of Hydrogen Using Earth-Abundant Metals: Showing Protons Around with Proton Relays. *Acc. Chem. Res.* **2015**, *48* (7), 2017–2026.
- (7) Fukuzumi, S.; Lee, Y. M.; Nam, W. Thermal and photocatalytic production of hydrogen with earth-abundant metal complexes. *Coord. Chem. Rev.* **2018**, *355*, 54–73.
- (8) Lubitz, W.; Ogata, H.; Rüdiger, O.; Reijerse, E. Hydrogenases. *Chem. Rev.* **2014**, *114* (8), 4081–4148.
- (9) Peters, J. W.; Schut, G. J.; Boyd, E. S.; Mulder, D. W.; Shepard, E. M.; Broderick, J. B.; King, P. W.; Adams, M. W. W. [FeFe]- and [NiFe]-hydrogenase diversity, mechanism, and maturation. *Biochim. Biophys. Acta, Mol. Cell Res.* **2015**, *1853* (6), 1350–1369.
- (10) Esselborn, J.; Muraki, N.; Klein, K.; Engelbrecht, V.; Metzler-Nolte, N.; Apfel, U. P.; Hofmann, E.; Kurisu, G.; Happe, T. A structural view of synthetic cofactor integration into [FeFe]-hydrogenases. *Chem. Sci.* **2016**, *7* (2), 959–968.
- (11) Wittkamp, F.; Senger, M.; Stripp, S. T.; Apfel, U. P. FeFe-Hydrogenases: recent developments and future perspectives. *Chem. Commun.* **2018**, *54* (47), 5934–5942.
- (12) Cornish, A. J.; Gartner, K.; Yang, H.; Peters, J. W.; Hegg, E. L. Mechanism of Proton Transfer in FeFe-Hydrogenase from *Clostridium pasteurianum*. *J. Biol. Chem.* **2011**, *286* (44), 38341–38347.
- (13) Hong, G.; Cornish, A. J.; Hegg, E. L.; Pachter, R. On understanding proton transfer to the biocatalytic [Fe-Fe]_H sub-cluster in [Fe-Fe] H₂ ases: QM/MM MD simulations. *Biochim. Biophys. Acta, Bioenerg.* **2011**, *1807* (5), 510–517.
- (14) Knörzer, P.; Silakov, A.; Foster, C. E.; Armstrong, F. A.; Lubitz, W.; Happe, T. Importance of the Protein Framework for Catalytic Activity of FeFe-Hydrogenases. *J. Biol. Chem.* **2012**, *287* (2), 1489–1499.
- (15) Long, H.; King, P. W.; Chang, C. H. Proton Transport in *Clostridium pasteurianum* FeFe Hydrogenase I: A Computational Study. *J. Phys. Chem. B* **2014**, *118* (4), 890–900.
- (16) Ginovska-Pangovska, B.; Ho, M. H.; Linehan, J. C.; Cheng, Y. H.; Dupuis, M.; Raugai, S.; Shaw, W. J. Molecular dynamics study of the proposed proton transport pathways in FeFe-hydrogenase. *Biochim. Biophys. Acta, Bioenerg.* **2014**, *1837* (1), 131–138.
- (17) Mulder, D. W.; Ratzloff, M. W.; Bruschi, M.; Greco, C.; Koonce, E.; Peters, J. W.; King, P. W. Investigations on the Role of Proton-Coupled Electron Transfer in Hydrogen Activation by FeFe-Hydrogenase. *J. Am. Chem. Soc.* **2014**, *136* (43), 15394–15402.
- (18) Mulder, D. W.; Guo, Y.; Ratzloff, M. W.; King, P. W. Identification of a Catalytic Iron-Hydride at the H-Cluster of [FeFe]-Hydrogenase. *J. Am. Chem. Soc.* **2017**, *139*, 83–86.
- (19) Silakov, A.; Wenk, B.; Reijerse, E.; Lubitz, W. ¹⁴N HYSCORE investigation of the H-cluster of FeFe hydrogenase: evidence for a nitrogen in the dithiol bridge. *Phys. Chem. Chem. Phys.* **2009**, *11* (31), 6592–6599.
- (20) Reijerse, E. J.; Pham, C. C.; Pelmenschikov, V.; Gilbert-Wilson, R.; Adamska-Venkatesh, A.; Siebel, J. F.; Gee, L. B.; Yoda, Y.; Tamasaku, K.; Lubitz, W.; Rauchfuss, T. B.; Cramer, S. P. Direct observation of an iron bound terminal hydride intermediate in [FeFe] hydrogenase. *J. Am. Chem. Soc.* **2017**, *139* (12), 4306–4309.
- (21) Pelmenschikov, V.; Birrell, J. A.; Pham, C. C.; Mishra, N.; Wang, H. X.; Sommer, C.; Reijerse, E.; Richers, C. P.; Tamasaku, K.; Yoda, Y.; Rauchfuss, T. B.; Lubitz, W.; Cramer, S. P. Reaction Coordinate Leading to H₂ Production in [FeFe] Hydrogenase Identified by Nuclear Resonance Vibrational Spectroscopy and Density Functional Theory. *J. Am. Chem. Soc.* **2017**, *139* (46), 16894–16902.
- (22) Pham, C. C.; Mulder, D. W.; Pelmenschikov, V.; King, P. W.; Ratzloff, M. W.; Wang, H.; Mishra, N.; Alp, E. E.; Zhao, J.; Hu, M. Y.; Tamasaku, K.; Yoda, Y.; Cramer, S. P. Terminal Hydride Species in [FeFe]-Hydrogenases are Vibrationally Coupled to the Active Site Environment. *Angew. Chem., Int. Ed.* **2018**, *57*, 10605–10609.
- (23) Rumpel, S.; Sommer, C.; Reijerse, E.; Fares, C.; Lubitz, W. Direct Detection of the Terminal Hydride Intermediate in FeFe Hydrogenase by NMR Spectroscopy. *J. Am. Chem. Soc.* **2018**, *140* (11), 3863–3866.
- (24) Lorent, C.; Katz, S.; Duan, J.; Kulka, C. J.; Caserta, G.; Teutloff, C.; Yadav, S.; Apfel, U.-P.; Winkler, M.; Happe, T.; Horch, M.; Zebger, I. Shedding light on proton and electron dynamics in [FeFe] hydrogenases. *J. Am. Chem. Soc.* **2020**, *142*, 5493–5497.
- (25) Seto, M.; Yoda, Y.; Kikuta, S.; Zhang, X. W.; Ando, M. Observation of Nuclear Resonant Scattering Accompanied by Phonon Excitation Using Synchrotron Radiation. *Phys. Rev. Lett.* **1995**, *74*, 3828–3831.
- (26) Chumakov, A.; Rüffer, R. Nuclear inelastic scattering. *Hyperfine Interact.* **1998**, *113* (1), 59–79.
- (27) Scheidt, W. R.; Li, J. F.; Sage, J. T. What Can Be Learned from Nuclear Resonance Vibrational Spectroscopy: Vibrational Dynamics and Hemes. *Chem. Rev.* **2017**, *117* (19), 12532–12563.
- (28) Hu, M. Y. Some notes on data analysis for nuclear resonant inelastic x-ray scattering. *Hyperfine Interact.* **2016**, *237*, 64.
- (29) Sage, J. T.; Paxson, C.; Wyllie, G. R. A.; Sturhahn, W.; Durbin, S. M.; Champion, P. M.; Alp, E. E.; Scheidt, W. R. Nuclear resonance vibrational spectroscopy of a protein active-site mimic. *J. Phys.: Condens. Matter* **2001**, *13*, 7707–7722.
- (30) Leu, B. M.; Zgierski, M. Z.; Wyllie, G. R. A.; Scheidt, W. R.; Sturhahn, W.; Alp, E. E.; Durbin, S. M.; Sage, J. T. Quantitative Vibrational Dynamics of Iron in Nitrosyl Porphyrins. *J. Am. Chem. Soc.* **2004**, *126* (13), 4211–4227.
- (31) Cramer, S. P. *Nuclear Resonance Vibrational Spectroscopy. In X-Ray Spectroscopy with Synchrotron Radiation: Fundamentals and Applications*; Springer International Publishing: Cham, 2020; pp 257–278.
- (32) Reijerse, E. J.; Pelmenschikov, V.; Birrell, J. A.; Richers, C. P.; Kaupp, M.; Rauchfuss, T. B.; Cramer, S. P.; Lubitz, W. Asymmetry in the Ligand Coordination Sphere of the [FeFe] Hydrogenase Active Site Is Reflected in the Magnetic Spin Interactions of the Azapropanedithiolate Ligand. *J. Phys. Chem. Lett.* **2019**, *10* (21), 6794–6799.
- (33) Berggren, G.; Adamska, A.; Lambert, C.; Simmons, T. R.; Esselborn, J.; Atta, M.; Gambarelli, S.; Mouesca, J. M.; Reijerse, E.; Lubitz, W.; Happe, T.; Artero, V.; Fontecave, M. Biomimetic assembly and activation of FeFe-hydrogenases. *Nature* **2013**, *499* (7456), 66.
- (34) Han, S.; Czernuszewicz, R. S.; Kimura, T.; Adams, M. W. W.; Spiro, T. G. Fe₂S₂ Protein Resonance Raman Revisited: Structural Variations among Adrenodoxin, Ferredoxin, and Red Paramagnetic Protein. *J. Am. Chem. Soc.* **1989**, *111* (10), 3505–3511.
- (35) Fu, W.; Drozdowski, P. M.; Davies, M. D.; Sligar, S. G.; Johnson, M. K. Resonance Raman and Magnetic Circular Dichroism

Studies of Reduced [2Fe-2S] Proteins. *J. Biol. Chem.* **1992**, *267* (22), 15502–15510.

(36) Birrell, J. A.; Pelmentschikov, V.; Mishra, N.; Wang, H.; Yoda, Y.; Tamasaku, K.; Rauchfuss, T. B.; Cramer, S. P.; Lubitz, W.; DeBeer, S. Spectroscopic and Computational Evidence that [FeFe] Hydrogenases Operate Exclusively with CO-Bridged Intermediates. *J. Am. Chem. Soc.* **2020**, *142* (1), 222–232.

(37) Schroer, C. G.; Agapov, I.; Brefeld, W.; Brinkmann, R.; Chae, Y. C.; Chao, H. C.; Eriksson, M.; Keil, J.; Nuel Gavalda, X.; Rohlsberger, R.; Seeck, O. H.; Sprung, M.; Tischer, M.; Wanzenberg, R.; Weckert, E. PETRA IV: the ultralow-emittance source project at DESY. *J. Synchrotron Radiat.* **2018**, *25* (5), 1277–1290.

(38) Custelcean, R.; Jackson, J. E. Dihydrogen Bonding: Structures, Energetics, and Dynamics. *Chem. Rev.* **2001**, *101* (7), 1963–1980.

(39) Klooster, W. T.; Koetzle, T. F.; Siegbahn, P. E. M.; Richardson, T. B.; Crabtree, R. H. Study of the N—H...H—B dihydrogen bond including the crystal structure of BH₃NH₃ by neutron diffraction. *J. Am. Chem. Soc.* **1999**, *121* (27), 6337–6343.

(40) Sanchez, M. L. K.; Sommer, C.; Reijerse, E.; Birrell, J. A.; Lubitz, W.; Dyer, R. B. Investigating the Kinetic Competency of CrHydA1 FeFe Hydrogenase Intermediate States via Time-Resolved Infrared Spectroscopy. *J. Am. Chem. Soc.* **2019**, *141* (40), 16064–16070.

(41) Sommer, C.; Adamska-Venkatesh, A.; Pawlak, K.; Birrell, J. A.; Rudiger, O.; Reijerse, E. J.; Lubitz, W. Proton Coupled Electronic Rearrangement within the H-Cluster as an Essential Step in the Catalytic Cycle of FeFe Hydrogenases. *J. Am. Chem. Soc.* **2017**, *139* (4), 1440–1443.

(42) Duan, J. F.; Senger, M.; Esselborn, J.; Engelbrecht, V.; Wittkamp, F.; Apfel, U. P.; Hofmann, E.; Stripp, S. T.; Happe, T.; Winkler, M. Crystallographic and spectroscopic assignment of the proton transfer pathway in FeFe-hydrogenases. *Nat. Commun.* **2018**, *9*, 4726.

(43) Ratzloff, M. W.; Artz, J. H.; Mulder, D. W.; Collins, R. T.; Furtak, T. E.; King, P. W. CO-Bridged H-Cluster Intermediates in the Catalytic Mechanism of FeFe-Hydrogenase CaI. *J. Am. Chem. Soc.* **2018**, *140* (24), 7623–7628.

(44) Arrigoni, F.; Bertini, L.; Bruschi, M.; Greco, C.; De Gioia, L.; Zampella, G. H₂ Activation in [FeFe]-Hydrogenase Cofactor Versus Diiron Dithiolate Models: Factors Underlying the Catalytic Success of Nature and Implications for an Improved Biomimicry. *Chem. - Eur. J.* **2019**, *25* (5), 1227–1241.

(45) Salna, B.; Benabbas, A.; Sage, J. T.; van Thor, J.; Champion, P. M. Wide-dynamic-range kinetic investigations of deep proton tunnelling in proteins. *Nat. Chem.* **2016**, *8* (9), 874–880.

(46) Greco, C.; Bruschi, M.; Fantucci, P.; Ryde, U.; De Gioia, L. Mechanistic and physiological implications of the interplay among iron-sulfur clusters in [FeFe]-hydrogenases. A QM/MM perspective. *J. Am. Chem. Soc.* **2011**, *133* (46), 18742–9.